

Design, construction and test of a prototype coil with demountable CuBe joints for pulsed table-top tokamaks

M. Lindero-Hernández^{a,*}, F. Trillaud^a, M. Nieto-Pérez^b, L.A. Montoya-Santianes^c and D. Hernández-Arriaga^d

^a*Instituto de Ingeniería, UNAM, CDMX 04510, Mexico.*

^{*}*e-mail: MLinderoH@iingen.unam.mx*

^b*Department of Nuclear Engineering, Pennsylvania State 16802, USA.*

^c*Universidad Politécnica de Querétaro, El Marqués, Querétaro 76240, Mexico.*

^d*Tecnológico Nacional de México, Campus Querétaro 76000, Mexico.*

Received 28 July 2023; accepted 12 October 2023

In a classic small tokamak, the magnetic confinement is achieved by toroidal coils that fit into a donut-shape mechanical structure. To facilitate their handling and maintenance as well as the access to various auxiliaries components, their design has evolved toward a modular configuration. For such demountable design, it is important to guarantee the electrical continuity of the winding of the coil across the modular parts through electrical contacts. The resulting joints rely on pressure and specific materials to transfer high current densities at a good mechanical stability and manageable losses. In the present work, a prototype of a circular demountable toroidal field coil (CDTFC) was designed and built to test some technical choices to be used in the final coils of a table-top tokamak referred to as TPM-1U. For this small tokamak, the magnet wires to wind the toroidal coils should be able to handle large pulsed currents in the tens of thousands of Amperes whereas the coil joints should handle a peak current density of at least 75 kA/cm². The case study here is the TPM-U1 table-top tokamak. Its conceptual design is recalled and mechanical and magnetic details of the demountable coil prototype are provided. For the experimental test, the contacts were slightly pressed using a custom-made contact assembly and current pulses between 4 kA and 8 kA were fed to the coil prototype. The degradation of the joint was visually estimated by assessing the amount of micro-melting, plastic deformation and oxidation appearing at the interface between the materials in contact. It is shown that the selected AWG-04 magnet wire is appropriate for carrying kilo-Ampere range pulsed currents and that the CuBe contacts are able to withstand current densities larger than the specification, up to 263 kA/cm², under low contact pressures of a few mega-Pascal simplifying their handling. Some technical choices have been probed on a prototype coil yielding a generic sequence of tasks to build and test mechanically and electromagnetically demountable coils and their joints.

Keywords: CuBe conical contacts; demountable coil; pulsed magnetic field; table-top tokamak.

DOI: <https://doi.org/10.31349/RevMexFis.70.021501>

1. Introduction

Demountable toroidal field coils (DTFC) have been actively developed to reduce the maintenance of tokamaks by facilitating their handling and the access to other components. Two modular concepts, static and flexible, have been commonly considered. The most typical joints are the static type which relies on solid Cu/Ag demountable contacts. These contacts have been employed in the spherical tokamak NSTX [1] to achieve a peak toroidal magnetic field of 0.3 T. For such a field strength, the electrical current is of the order of 36 kA with a contact pressure of about 5.5 MPa. To improve the electrical contact, Ag-coating is often used as in the case of the cylindrical Z-pinch plasma machine [2]. Besides static contacts, there is the option to utilize some flexible connections even though they are less common. These contacts can conduct large amount of current up to 18 kA to achieve a toroidal magnetic field of about 0.7 T [3]. They are particularly relevant to produce large enough pulsed fields for sustaining short-time stable plasma employing resistive coils. However, for bigger tokamaks such as the ARIES-I of a sizable 6.75 m in radius [4], the conventional coils are not

practical to transfer electrical currents between a few mega-Amperes and tens of mega-Ampere (24 MA for ARIES-I) to reach magnetic flux densities in the Tesla range. Therefore, alternative technologies using superconductors are required to handle the intense current densities at negligible losses or no losses. In this case, the aforementioned contacts become unsuitable as the system should be maintained at cryogenic temperature in a tight vacuum. Lately, REBCO technology has triggered undeniable interest as this high temperature superconductor (HTS) can withstand large intensities of applied magnetic field without losing the bulk of its transport current capability [5]. For instance, it has been considered for the vulcan tokamak (YBCO, reactor radius equal to 1.2 m) and the FFHR-1d helicoidal reactor (GdBCO, major radius of helicoidal coils equal to 15.6 m). The vulcan tokamak is to be operated at 2.3 MA to yield a toroidal magnetic field up to 7 T with DTFC segmented at their midplane allowing the dismantling of the primary vacuum chamber [6]. The FFHR-1d is designed for 91 kA providing magnetic toroidal fields up to 4.6 T. For the latter, the joint sections are fabricated with mechanical bridge joined tapes [7]. Despite the sensitivity of the HTS to high-energy neutron radiation, the gain in center field

is expected to be substantial, up to 20 T such as in the proposed ARC tokamak [8]. Nowadays, HTS demountable coils for large scale fusion reactors such as ITER and SPARC, are being constructed [9, 10]. This modular design enable their transportation and assembly *in situ* to target a fusion gain Q larger than 1. ITER uses low temperature superconductors (LTS) as they are more widely used and rely on decades of experience such as the Nb_3Sn and the NbTi . These are shaped into cable-in-conduit conductors to transmit 68 kA at 5.3 T center field with demountable toroidal joints [9]. However, in the case of SPARC, REBCO is expected to transmit 41 kA at 12 T difficulty reachable by LTS [10].

As understood from these different technologies, to achieve the desired field magnitudes, materials that can sustain high current densities are utilized to their limits bearing in mind an adaptable structural design. In that regard, demountable concepts are ubiquitous in the design of fusion magnets integrating joints capable of working under high current densities, low contact resistances and low contact pressures regardless of the conductor technology.

In the present work, a conventional technology is considered for a small tokamak referred to as TPM-1U. This small tokamak made of conventional DTFC or CDTFC should provide a magnetic flux at the coil center of 1 T. A prototype of CDTFC with conical CuBe (C172) joints wound with 4 turns of Cu magnet wire (AWG-04) has been designed, built and tested. The joints, that should transmit at least 75 kA/cm^2 , have been previously studied at low contact pressures [11]. The present work follows a preliminary study carried out in Ref. [12]. Additional tests have been conducted under light clamping pressure and additional tests have been carried out to check the technological choice made to build the demountable coil.

This paper is organized as follows. The Sec. 2 recalls the basic design considerations taken for the conventional TPM-1U table-top tokamak and the choice of CDTFC. The subsequent Sec. 3 presents the design and construction of the CDTFC prototype to be tested. Some mechanical and electrical tests have been performed to validate some technical choices. This section present the CuBe conical contacts as well. The next Sec. 4 corresponds to the different tests involving the CDTFC prototype and its joint under pulsed currents. Here, the pulsed magnetic field is measured at the center axis of the coil allowing to reconstruct its actual current and compare it to the specification. Finally, the Sec. 5 concludes the present work. Besides the validation of the CDTFC design proposal for a table-top tokamak, it is shown that conical CuBe contacts are suitable for transferring repeated current densities up to 75 kA/cm^2 without noticeable damages. An important step in the development of durable joints with easy handling for fast and reliable assembly and disassembly.

2. TPM-1U design

In the present section, the conceptual design of the TPM-1U tokamak is briefly recalled that lead to the choice of CDTFC.

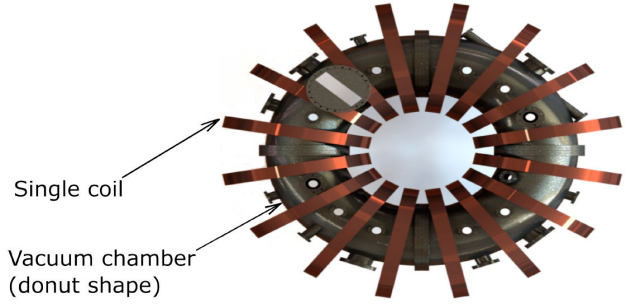


FIGURE 1. Overview of the TPM-1U tokamak showing the distribution of 16 CDTFC around the vacuum chamber.

TABLE I. Design parameters of the TPM-1U.

Design parameter	Symbol	Value
Major radius	R	0.4 m
Minor radius	a	0.15 m
Central Magnetic Field	B	0.5 to 1.0 T
Plasma current	I_p	25 to 50 kA
Central electron density	n_e	$1 \times 10^{19} \text{ m}^{-3}$
Central electron temperature	T_e	300 eV
Pulse time duration	τ	10 to 30 ms

It allows introducing the requirements that the CDTFC should fulfill to provide the required field. Table I presents the specifications of the TPM-1U. TPM-1U is made of 16 CDTFC following a donut-shape structure [13]. It makes use of conventional coils wound with insulated Cu magnet wires. Despite the growing interest in HTS, they are still more suitable than superconductors for building a small table-top pulsed tokamak to supply of the order of 1 T on axis. There is still some incentive to build such a small system, in particular, to study specific technologies, even HTS, on a cheap sub-scale device. In the present case, the Tesla-range pulsed field lasts for 30 ms. To do so, the Pulse Forming Network (PFN) is used as proposed in Ref. [14]. Figure 1 shows an overview of the TPM-1U tokamak. For such a device, the CDTFC have an inner diameter D equal to 0.5 m. The design is such that the field ripple Ψ is at most 2.5%. The ripple is computed as $\Psi = (B_{\max} - B_{\min})/B_{\max}$, where B_{\max} and B_{\min} are the maximum and minimum magnetic flux densities, respectively. The geometrical centers of the toroidal coils lie on a circle in the equatorial plane centered in the origin, with a radius larger than the torus major radius by a factor of ΔR . In the present case, the ripple can be controlled by varying ΔR as seen in Fig. 2; ΔR is defined as the difference between the major radius of the toroidal coil R_o and the major radius of the plasma column R_p ($\Delta R = R_o - R_p$). In [14], considering a shift ΔR of the coil going from 0.04 m to 0.07 m, a magnetic field ripple below 5 % can be achieved. The maximum magnetic field ripple will occur along the circumference that defines the torus outer edge in the equatorial

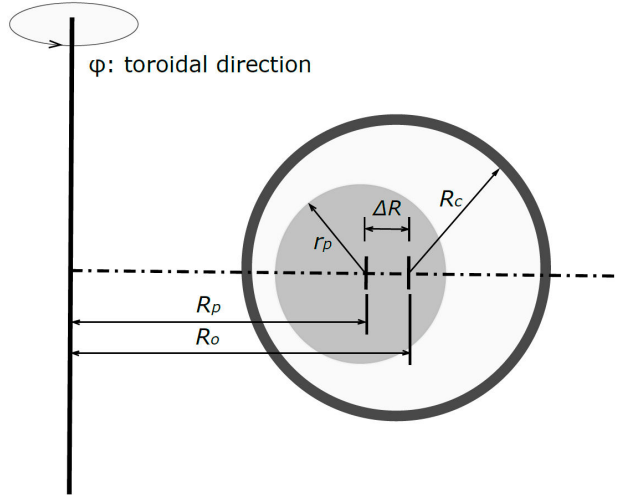


FIGURE 2. Cross section of the tokamak showing the plasma column inside the TF coil and the relevant geometric parameters.

plane. The maximum field on the circumference, B_{\max} , follows the toroidal angle that corresponds to a plane defined by a toroidal coil. The minimum field, B_{\min} , follows the toroidal angle defined by a vertical plane that bisects the region delimited by two adjacent toroidal coil planes.

The magnetic field is greater in the central part than in the outer part. Due to the coil separation in the peripheral region the intensity of the magnetic field varies which produces a ripple in the intensity of the magnetic field. These field disturbances are unavoidable, and to reduce their effect a great number of coils are often implemented. However, for small experiments, space restriction is a strong limitation. Therefore, to counteract the asymmetric field variation over a magnetic surface some practical techniques in coil design have been proposed as presented in Ref. [15]. The techniques consist in the use of oversized coils in some extent to improve the field symmetry but in other cases the field variation may be reduced by implementing segmented coils and increasing the currents adjacent to the access gaps. More conservative and somewhat desirable tolerances are also proposed with ripples of less than 1.5 % as discussed in Ref. [16]. In the present case, a convenient balance is found between the size of the tokamak given by the number of coils and the homogeneity of the field by choosing the ripple criterion to be 2.5 %. This criterion is particularly important as it yields the overall size of the tokamak. The net toroidal magnetic field of the 16 coils goes from 0.5 T to 1.0 T while the reported value of ~ 0.1 T is only for the single coil tested here. The proposed magnetic field of 0.1 T for the 4-turn single coil is to test its behaviour under currents with the same order of magnitude than those of the multi-turn coil. The latter is designed to work in the range between 0.5 T and 1.0 T. The prototype 4-turn coil tested in this article is similar in size and carries similar currents than the final multi-turn coil. This final coil would be capable to produce the toroidal magnetic field in the range of 0.5 T to 1.0 T. Here, the evaluation of the demountable coil with few

TABLE II. Plasma column and coil parameters of the TPM-1U.

Design parameter	Symbol	Value
Coil major radius	R_o	$\Delta R + R_p$
Coil minor radius	R_c	0.25 m
Plasma edge radius	r_p	0.1 m
Plasma column center	R_p	0.45 m
Shift	ΔR	0.04 m to 0.07 m

turns is a first step for designing coils of more turns while keeping currents around ~ 12 kA to reach 1.0 T.

For the TPM-1U tokamak, the CDTFC have a circular shape that are adequate for compact, small tokamaks with low field in the range of a Tesla since they have simple and low-cost designs. For a target field and coil dimensions and numbers given by the size of the tokamak, the choice of the wire magnet arises from computing the amount of current in a coil. The starting point is the estimation of the total current in the tokamak to produce a given plasma. The following equation relates the key features of the plasma dimensions to the total current,

$$I_c = \frac{qR_cR_p}{r_p^2|F(r_p)|} I_p. \quad (1)$$

For the TPM-1U, the plasma edge radius r_p is 0.1 m with a radius of the plasma column center R_p (defined by the available vacuum vessel) equal to 0.45 m. The geometrical factor $|F(r_p)|$ is 2.25, and the coil minor radius R_c is 0.25 m. The geometrical parameters of the coil and the plasma column are reported in Table II; these dimensions ensure there are no interferences between coils, vacuum vessel and plasma column, and that the plasma column is adequately contained within the vessel.

By choosing the safety factor $q(r_p)$ equal to 3 according to [14] and considering that $I_c \cong 15I_p$, the total Ampere-turns in the tokamak should be equal to 750 kA [14]. Knowing the total current and choosing the amount of CDTFC to be 16 in the present design, the following configuration is proposed with each coil holding 8 layers made of 8 turns of magnet wire per layer leading to 12 kA per turn for a total current of 768 kA fulfilling the total number of Amper-turns. Assuming 12 kA, the Cu wire gauge is computed based on the Onderdonk's equation (2) given by,

$$I_f = \sqrt{\frac{A^2}{33t} \ln \left(\left[\frac{T_m - T_a}{234 - T_a} \right] - 1 \right)}. \quad (2)$$

This equation yields the current I_f at which the Cu wire melts in steady state [17]. For the calculation, the coil current I_c , and the pulsed time t_p are 15 kA and 32 ms, respectively. These values are larger than the actual specifications for the TPM-1U for safe operation. Knowing that the melting temperature of copper T_m is equal to 1,353 K and if one assumes an ambient temperature T_a of 300 K, the wire gauge for the

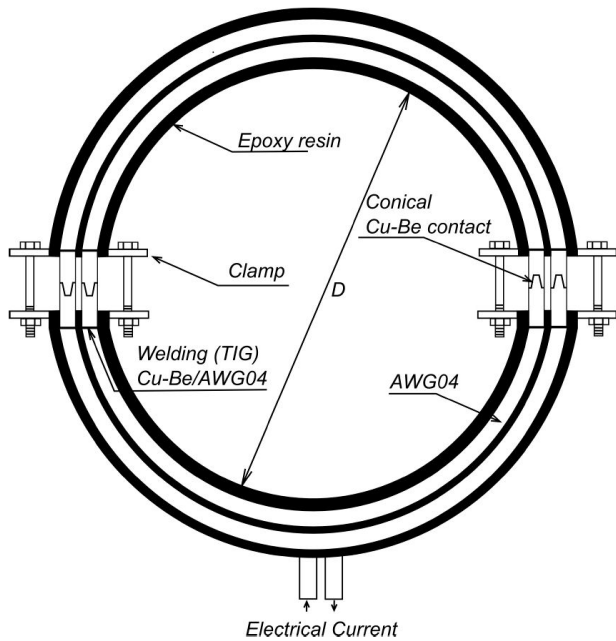


FIGURE 3. CDTFC schematic drawing showing the CuBe conical contacts welded to the AWG-04 magnet wires. Clamps are used to fix the conical contacts. The coil is impregnated with epoxy resin.

TABLE III. CDTFC Parameters (see Fig. 3).

Design parameter	Symbol	Value
Number of turns	N	4
Target center field	B	0.1 T
Inner diameter	D	0.39 m
Wire diameter	d	5.2×10^{-3} m
Separation between turns	δ	3×10^{-3} m
Estimated current for 0.1 T	I	8.04 kA
Coil inductance	L	13.4 μ H

magnet wire is found to be AWG-08. An additional safety margin is taken. The final gauge is AWG-04 guaranteeing a robust operation of the pulsed tokamak. The coil is wound on a support made of a polyacetal cylinder whose inner diameter is 0.39 m. Additionally, two straight sections of 0.06 m long are machined in the core periphery to facilitate the welding of the contacts in place as shown in Fig. 3. The Table III summarizes the salient parameters of the CDTFC for the TPM-1U tokamak. In the next section, a prototype of the CDTFC is introduced. It is a sub-scale of the actual CDTFC to be used in TPM-1U. Nonetheless, the requirements in terms of current and field are similar. It was purposely designed to test the resiliency of the magnet wire and the demountable joints to pulsed currents of the order of 10 kA. The specification of the joints is the repeated handling of current densities of at least 75 A/cm^2 without visible degradation.

3. Design and tests leading to the construction of the CDTFC prototype

In the following section, the steps taken to design the coil prototype are detailed including mechanical, electrical and magnetic aspects. Some tests were performed to check the technological choices. Ultimately, this design shall be used for the final coils.

3.1. Overview of the coil prototype for testing

The CDTFC prototype is made of 4 turns of AWG-04 magnet wires. Table III gives the design parameters of the coil prototype. For the test, the target center field is 0.1 T. The current is estimated assuming a simple filamentary current loop as follows,

$$I = \frac{DB}{\mu_0 N}. \quad (3)$$

As aforementioned, the CDTFC prototype for testing is smaller than the final coil used in the TPM-1U tokamak. The tests are conducted to check two specific aspects: 1) the ability of a CDTFC wound with AWG-04 magnet wires to handle transport current up to 10 kA and 2) the capability of the demountable joint to sustain at least 75 A/cm^2 .

The subsequent sections present some technical choices made for the CDTFC prototype with details of the electrical contacts. Some specific tests to warrant those choices were carried out and are reported hereafter.

3.2. Mechanical considerations for the CDTFC

For small tokamaks with moderate fields (of the order of 1.0 T) the forces developed between the coils remain small and can often be easily taken on by a metal shell encapsulating coils impregnated with epoxy. The epoxy resin avoids the relative movements between conductors guaranteeing field stability and mechanical strength. Typically, the most largest forces are found between consecutive turns. These forces compress the turns together. According to Akyel [18], the main component of the force is found along the z axis of the coil. The forces in the x - y plane are typically 60 times smaller. Hence, for a preliminary design, only the force F_z has been taken into account in the present study.

To reduce the force exerted between turns, the turns are separated by a 3 mm wide gap using plastic crosses every few centimeters. In addition to their structural purpose, these separations also avoids short circuits that had occurred in past tests. The next subsection introduces some mechanical and dielectric tests conducted on the epoxy impregnation to check the mechanical strength and dielectric strength of the binding material.

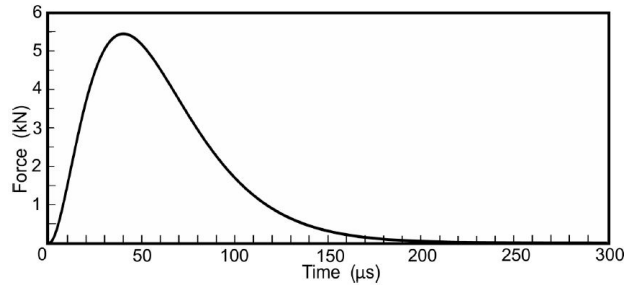


FIGURE 4. Evolution of the peak F_z vertical force developed between turns. A maximum current pulse of 8.2 kA for 220 μs flowed through the coil producing a maximum force equal to 5.5 kN.

3.3. Mechanical and dielectric tests on epoxy resin

The force F_z is solved using the magnetic model developed in Subsec. 4.2. It takes the following expression,

$$F_z = \frac{\mu_0 I^2 k \delta}{4R} \left[2K(k) - \left(\frac{2-k^2}{1-k^2} \right) E(k) \right], \quad (4)$$

where k is a dimensionless variable related to the mean radius R of the coil and their separation δ according to,

$$k = \frac{2R}{(4R^2 + \delta^2)^{0.5}}, \quad (5)$$

where $K(k)$ and $E(k)$ are the complete elliptic integrals of the first and second kind [19,20], respectively. In order to estimate F_z experimentally, a current pulse of 8.2 kA peak for 200 μs was applied to the CDTFC. The response is shown in Fig. 4. Taking the maximum force equal to 5.5 kN and dividing it by the projected area of a single turn $A_t = \pi D_a d$, with $D_a = 0.4$ m and $d = 0.005$ m, an estimated axial stress of $\sigma \sim 0.9$ MPa is calculated. In compression, the level of stress is manageable by any common epoxies. Here, the standard epoxy resin RE-7001 was chosen despite the few information provided by the manufacturer. Nevertheless, to ensure that the resin can handle the stress in operation, some epoxy samples have been prepared and tested following the standard tensile test for polymers ASTM D638 Type 1. For this test, they have a cross section area $A_s = 0.005 \times 0.007$ m. The normalized samples are shown in Fig. 5. The tensile result is given in Fig. 6. It should be noted that the formation of air bubbles is unavoidable during the preparation of the samples. These bubbles are responsible for the reduction of the mechanical resistance of the samples to deformation. The cross section of a set of cured samples were inspected to identify the presence and characteristics of trapped air bubbles. The diameter of the air bubbles were less than 0.5 mm. To account for the presence of bubbles, various samples were tested to provide an average on the maximum force handled by the samples in tensile test before plastic deformation. In the present case, the average maximum force F_{emx} reached before the onset of the plastic deformation is 454 N leading to an average maximum elastic stress σ_{emx} equal to about

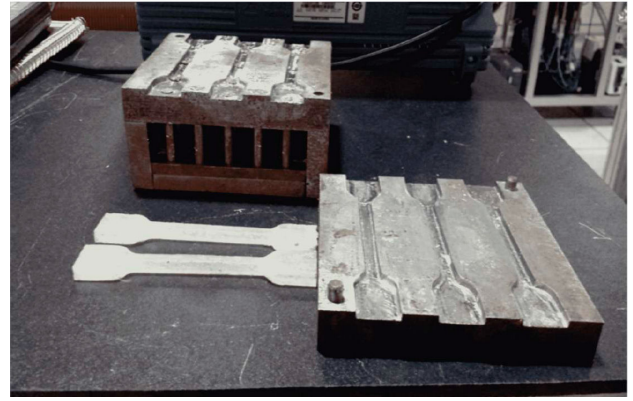


FIGURE 5. Standardized samples made with RE-7001 resin to be characterized under tensile tests.

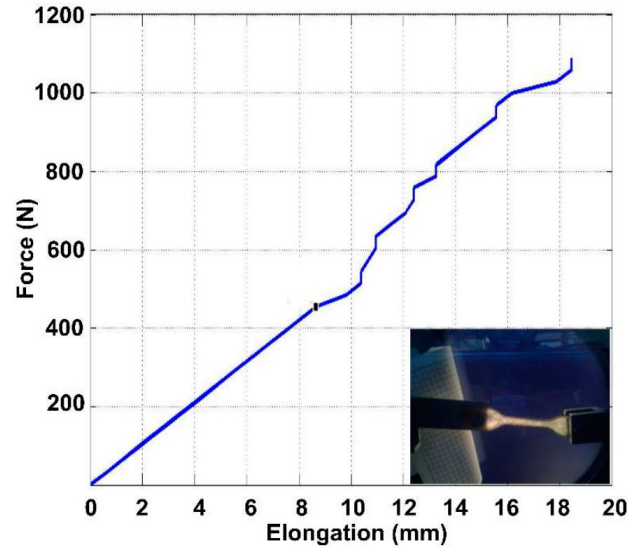


FIGURE 6. Force versus elongation graph for RE-7001 resin samples during stress testing.

13 MPa. Here, the average maximum elastic stress was computed by dividing the average maximum force F_{emx} by the cross section area of the material (gauge length section of the sample). The ratio between the average maximum elastic stress for the resin (13 MPa) and the estimated axial stress (0.9 MPa) is around 14 indicating that the resin RE-7001 may be subjected to over-stresses under magnetic field greater than 0.1 T therefore deforming either plastically or simply break.

Besides the mechanical tests, some additional tests on the dielectric strength of the resin were carried out. Square sheets (3 \times 3 cm) of epoxy with a thickness of 1 mm were subjected to a constant voltage of 8 kV for 3 minutes without voltage breakdown yielding a conservative dielectric strength taken as 8 kV/mm.

3.4. Choice of design and material for electrical contacts between coil sections

Copper and copper alloys are common materials to manufacture coils [21]. For relatively low field target, they can carry the pulsed current without overheating as a result of their good overall thermal and electrical properties at a relative low cost. In the present case, as the toroidal magnetic field of the TPM-1U is moderate for a table-top tokamak, the current density and resulting heating in the coils can be properly handled without particular issues. Nevertheless, there is still the need to evaluate the joint design, its weldability, mechanical resistance, electrical and thermal conductivity to ensure the proper transfer of energy between the coil sections. The design should also guarantee that it has a negligible effect on the magnetic field uniformity. Indeed, as discussed in Ref. [4] for the specific case of ARIES-I, there is no assurance that the demountable coil geometry would provide the same field uniformity as a continuous configuration. It is expected that local magnetic field distortions at the joints may arise due to the difference in resistance between the two contacts thereby disrupting the current flow. This effect can be mitigated with the right choice of contact materials providing low electrical resistance at high current density capacity. For the current project, the attention has been focused on CuBe (C172) contacts. A previous study reported in Ref. [11] was performed on such joints varying the contact pressure and the cross section area to look for degradation. It was found that the application of relative low contact pressures may increase the probability of local melting at the interface between the CuBe / CuBe joint. The contact melting in pulsed regime has not been treated widely. It was originally thought that increasing the contact pressure allows transmitting more current density at a lesser risk of melting. The nature of the contact resistance varies during the pulse experiment and depends on the pressure exerted in each electrical contact as demonstrated in Ref. [1, 22]. In Ref. [22], experiments were conducted on pure Al-Cu contacts under a pressure of 6 MPa for a current density of 56 kA/cm² where local melting occur leading to the degradation of the contact. The melting was between a single pair of Al / Cu contacts. It was shown that it could be suppressed by applying 27 MPa for a current density of 57 kA/cm². Homogeneous pressure distribution is relatively easy to achieve for a single contact configuration but not for demountable coils whose multi-contact arrangement rises the probability of contact failure. Such failure has been identified in the toroidal field coil of the NSTX where a static contact (silver plated copper) detached opening the joint during operation eventually causing a plasma arcing [23]. Materials like copper and aluminum require a threshold pressure to avoid melting; however, silver plated copper, in the NSTX case, locally melted due to the constricted high current density over small contact surfaces as these contacts opened up for a current of 50 kA. The probability of such failures can be lessened for the CDTFC by means of conical contacts. The conical shape allows to conserve a large contact surface even

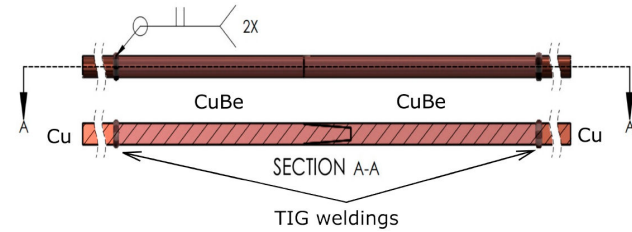


FIGURE 7. Details of the CuBe/CuBe joint ensuring the electrical continuity from one Cu wire (AWG04 insulated magnet wire) of one coil section to another Cu wire belonging to the second section. Self-aligned conical contacts providing good mechanical stability with a high contact area of $\sim 0.29 \text{ cm}^2$.

though, under the influence of bending moments induced by non-axial external forces, the joint may deform. Consequently, it could allow a wider tolerance to withstand high current densities than flat contacts. To see if such effect may arise in CuBe conical contacts, we chose the same procedure as in Ref. [22] but over a broader range of pressures and current densities: 263 kA/cm² under 66 MPa and 131 kA/cm² under loose contact. In this large interval of tests, no melting and general degradation was visually observed making CuBe (C172) a valid candidate for low pressure and high current density joints. As the pressure is decreased and the risk of melting lessens still procuring a good electrical contact, the joint design drastically simplifies. Finally, straight CuBe contact sections were selected with conical geometry to maximize the contact area to pass the same amount of current between turns but at a lower current density. The advantages of conical contacts are twofold: 1) low current density therefore less heating, 2) increase of mechanical stability at relative low contact pressures by providing a self mechanical alignment with good electrical contact. The conical contact is illustrated in Fig. 7. One Cu wire (AWG04 insulated magnet wire) from one section of the coil is soldered to the male contact and another to the female contact; this for all the turns of the coil. To maintain all the contacts in place, a mechanical structure was built to clamp the two sections of the coil. The coil with the joint are then impregnated by epoxy. Details of the clamping are given in Subsec. 3.5.

3.5. CDTFC assembly

A pre-support of the conical CuBe/CuBe joints was used for the impregnation process before being replaced by the final, more sophisticated, clamping structure to hold in place the joints for handling and coil operation. The pre-support is assembled using hex socket headless screws and parallel screws as given by the figure inserted into Fig. 8. This pre-support provides a small pre-compression to keep the electrical contacts in contact, no relative motion between the female and male parts, during the coil impregnation. This epoxy impregnation is done in a wood mold as shown in Fig. 8. Wax paper was employed to ease the dismantle of the coil from its mold. Hardened white plasticine stops the resin from passing over to the demountable sections. At the end of the process, a

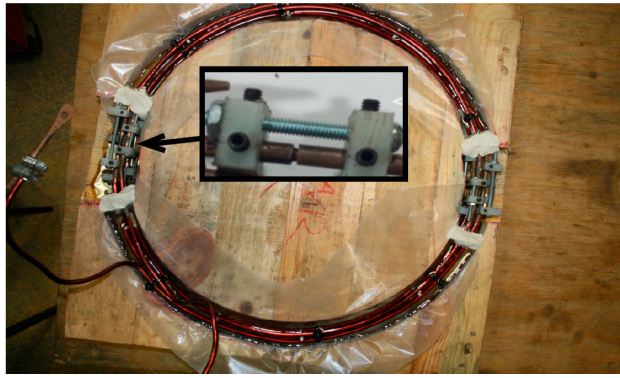


FIGURE 8. Fastening system to press the conical CuBe contacts together before the epoxy impregnation of the coil. The CDTFC lies in its wood mold.

TABLE IV. Material properties.

Material	Components	Young's		
		Mod. (GPa)	Poisson's Ratio	Density (kg/m ³)
Copper Alloy	Male	110	0.34	8300
	Female			
Contacts				
Epoxy Resin	Resin Blocks	3.78	0.35	1170
Structural Steel	L pieces	200	0.3	7850
	Bolts			
	Nuts			

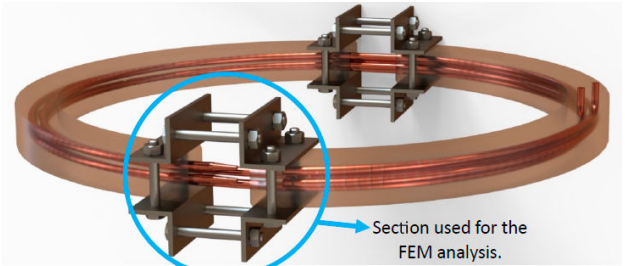
simple electrical continuity test was conducted to ensure that there were no false contacts or open circuit.

The CDTFC encapsulation is carried out slowly to reduce the amount of air bubbles. No vacuum impregnation system was available at the time. A period of 24 hours is the average time to cure the epoxy resin. Once the epoxy resin has hardened, the screws are removed to unfasten the conical CuBe male-female contact tips. As described in Subsec. 3.4, the CuBe joint can work even at low pressures, thus it allows in principle the implementation of a relative simple clamping system to fasten the two CDTFC halves. This clamping system can be seen on the final coil whose picture is given by Fig. 9a). Four “L” shaped angle steel pieces are used in its assembly to provide a pressure of ~0.5 MPa. This pressure is sufficient to maintain in place the joints during the handling and operation of the coil.

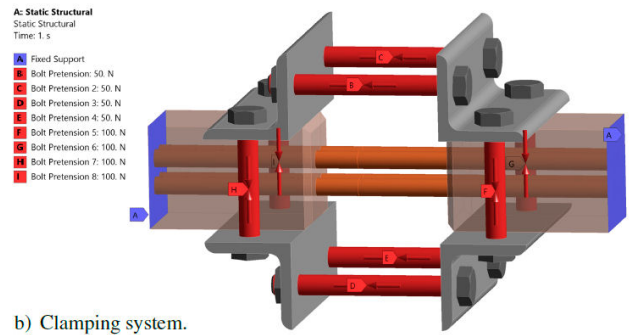
The next section presents a static mechanical analysis to ensure that the clamping structure complies with its function without damaging the joints.

3.6. Static mechanical analysis of the clamping structure

The clamping structure as well as the conical CuBe joints are studied via a static structural analysis conducted in ANSYS



a) CAD of the CDTFC.



b) Clamping system.

FIGURE 9. CAD of the CDTFC. a) details of the clamping system, b) Positioning of pre-loading and fixed supports.

Workbench. The maximum mechanical load withstood by the materials is determined. Figure 9 presents the entire coil assembly. Figure 9a) illustrates the demountable coil and the clamping structure. The clamping structure to hold the joints is detailed in Fig. 9a).

For this analysis, there is no current flowing through the system. The female and male contacts are embedded in two separated blocks of epoxy resin allowing relative motion between them which corresponds to the worst case scenario. The clamping structure is made of four pieces of structural steel having a “L” shape. M6 bolts and nuts were used to hold the “L” pieces in place. The properties of these materials can be found in Table IV. The average maximum elastic stress estimated experimentally in Subsec. 3.3, equal to 13 MPa, was used as tensile yield strength for the resin. The condition of bonded contacts without sliding and separation between the edges and faces of all the parts in contacts were incorporated in the model. The resin blocks and the bolts were meshed using hexahedrons while tetrahedrons were used for the wire. The lateral end faces of the resin blocks including the end faces of the contact wires were considered as fixed supports, see Fig. 9a). In the present study, the mechanical analysis was used to determine the pre-tension on the bolts to ensure a proper clamping without damaging the epoxy and losing the electrical contacts at the joints. The pre-tension was incrementally increased until the yield strength of the resin was reached or the contact separated. Ten steps were run. The computation time for each step was about one second. The pre-tension values used on the horizontal bolts, in the same direction as the coil wire, and on the vertical bolts, perpendicular to the wire, are shown in Table V. By applying a larger

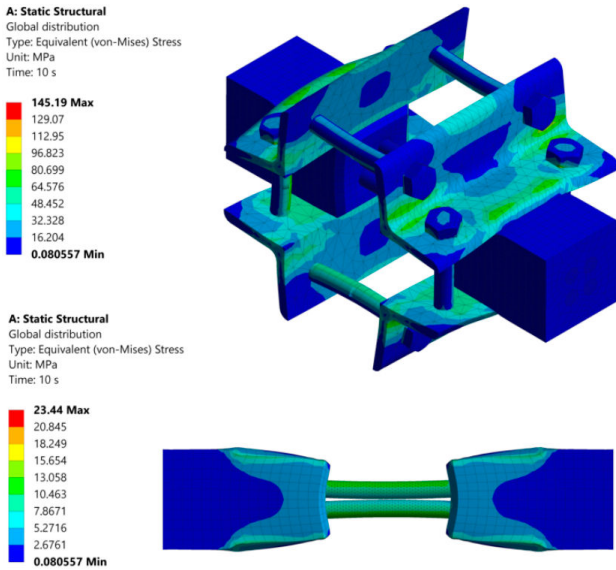


FIGURE 10. Global distribution of the resulting stresses.

TABLE V. Pre-tension steps used and maximum stress developing in the resin block.

Step (s)	Horizontal Bolts (N)	Vertical Bolts (N)	Maximum Stress (MPa)
1	50	100	1.42
2	100	200	2.84
3	150	300	4.26
4	200	400	5.67
5	250	500	7.09
6	300	600	8.51
7	350	700	9.92
8	400	800	11.34
9	450	900	12.76
10	500	1000	14.17

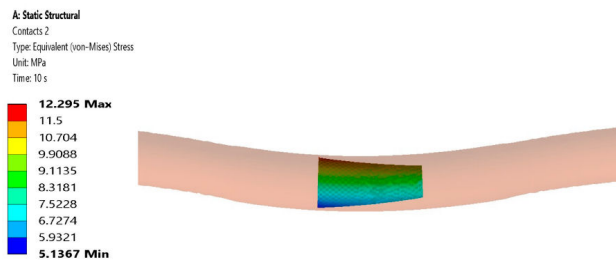


FIGURE 11. Stress distribution in the male section of two parallel conical contacts.

pre-tension on the vertical bolts than on the horizontal ones, it is possible to avoid any relative horizontal movement between the “L” pieces and the epoxy resin blocks. The result of the global distribution of equivalent von-Misses stresses in the different components of the assembly is shown in Fig. 10. A scale factor of 0.5 was applied to the deformation.

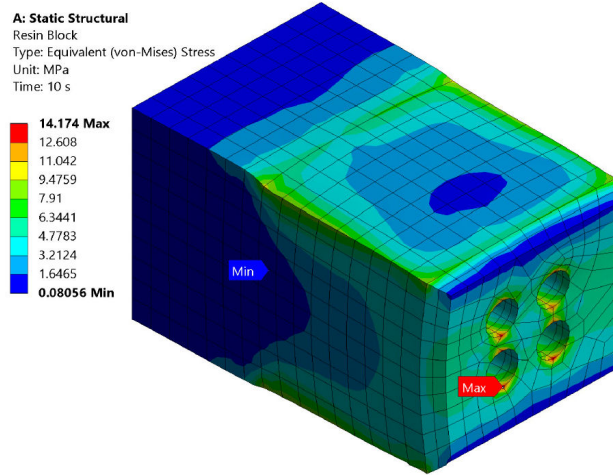


FIGURE 12. Stress distribution in the resin block.

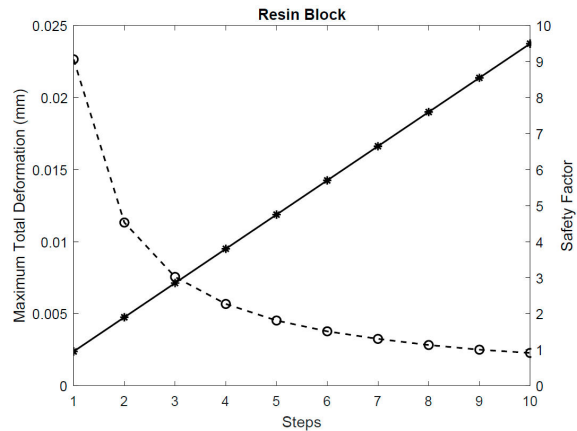


FIGURE 13. Maximum total deformation and safety factor in the resin block.

Since the forces exerted in the male-female conical contacts are of the same magnitude but opposite in direction, only the force exerted by the female contact on the male one is shown in Fig. 11. The load transfers from the clamping causes a bending moment in the cross section of the conical contacts. The peak stress values including all bolt pre-tensions given in Table V range from 1.22 MPa to 12.29 MPa.

The maximum equivalent stress in the resin block increases when the load increases as shown in Table V. The maximum stress varies linearly with the load until it reaches a value of 14.17 MPa. These values are concentrated at the interface between the resin block and the wire of the male-female contacts. The surface contact area between each “L” piece and the resin block did not show greater stresses than those present between the resin block and the wire of the male-female contacts, up to 10.14 MPa. The changes in the maximum total deformation and the safety factor as the load values for the resin block are increased as shown in Fig. 13. The safety factor was used as a measure to evaluate the structural resistance of the resin block. It is defined as the ratio between the yield stress of the material over the equivalent maximum stress given by the model. The total deformation

increases until reaching a value of 0.023 mm as the load increases, while the safety factor decreases from 9.06 to 0.91.

Considering the behavior in the characterization of the resin in Sec. 3.3, it is not expected to observe the typical pattern with the hardening and necking sections for ductile materials. Indeed, the resin behaves more brittle than ductile and the possibility of a fracture can be assumed. Therefore, for the last pre-load values (step 10) the resin blocks is likely to have yielded or fractured. Hence, for safety, step 7 with a maximum stress equal to 9.92 MPa provides the forces to apply to the vertical and horizontal bolts to ensure clamping without damaging the resin or loosening the contacts. It is important to mention that the stresses at the junctions were obtained through simulation only.

4. Electric and magnetic tests performed on the CDTFC

4.1. Electrical tests under pulsed current

Figure 14 shows the circuit used to supply the pulse of current to the CDTFC. A voltage source V charges a high-voltage capacitor bank C . The capacitor bank discharges into the CDTFC simulated by a resistance R_{coil} in series with an inductance L . Previous experiments were conducted to estimate the inductance and resistance of a continuous 4 turn coil (without CuBe contacts). The experimental circuit was similar to the one shown in Fig. 14. For these experiments, the current given in Fig. 15 followed the expression $I = 8.9547e^{-\alpha t} \sin(\omega t)$ corresponding to the experimental oscillatory pulse provided in Fig. 15, with $\alpha = 10350 \text{ s}^{-1}$ and $\omega = 29920 \text{ rad/s}$. Repeating the measurements and taking into account the resistance and inductance of the cables ($R_{par} = 0.353 \text{ } \Omega$ and $L_{par} = 3.7 \times 10^{-6}$), from the inverse of the time constant $\alpha = R_{Tot}/2L_{Tot}$ (R_{Tot} : total resistance and L_{Tot} : total inductance) and the pulsation $\omega = \sqrt{1/(L_{Tot} * 58.5 \times 10^{-6}) - \alpha^2}$, the resultant inductance and resistance for the coil is $L_{coil} = 13.4 \text{ } \mu\text{H}$ and

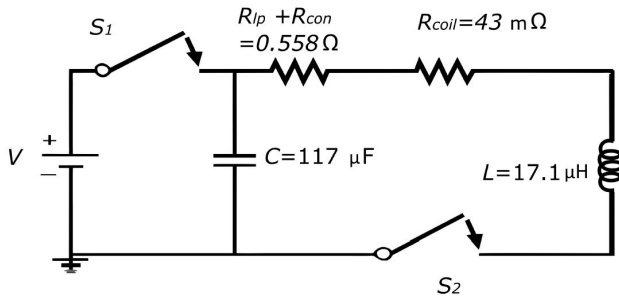


FIGURE 14. Circuit diagram for generating the pulsed currents. A high voltage power supply V charges at 7.5 kV a capacitor bank $C = 117 \text{ } \mu\text{F}$ that discharges a pulsed current in the circuit made of the resistance $R_{lp} + R_{con} = 0.55 + 0.008 \text{ } \Omega$ and the coil simulated as a resistance $R_{coil} = 0.043 \text{ } \Omega$ and an inductance $L = 17.1 \text{ } \mu\text{H}$. The resistance R_{lp} encompasses all the connection and cabling resistances plus a limiting resistance; R_{con} represents the joints' resistance.

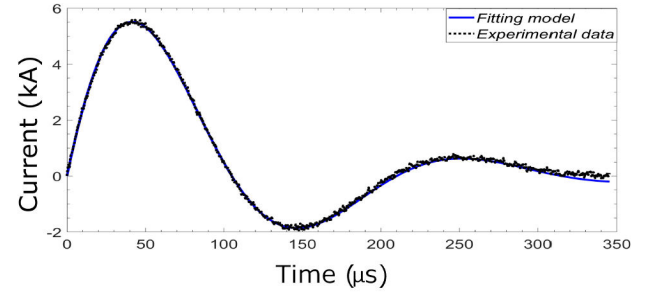


FIGURE 15. Oscillatory current pulse to calculate the inductance and resistance of the 4 turn continuous coil. Fit of the data: $I = 8.9547e^{-\alpha t} \sin(\omega t)$, with $\alpha = 10350 \text{ s}^{-1}$ and $\omega = 29920 \text{ rad/s}$.

$R_{coil} = 0.043 \text{ } \Omega$, respectively. The resistance R_{lp} represents an equivalent resistance combining all the connection and cabling resistances plus a limiting resistance to fix the maximum current in the circuit. The resistance R_{con} corresponds to the resulting resistance of all the CuBe joints. The switches S_1 and S_2 command the charge ($S_1 = 1, S_2 = 0$) and discharge ($S_1 = 0$ and $S_2 = 1$) of the capacitor bank. S_1 is a common switch with voltage and current characteristics of 127 V and 10 A, respectively. S_2 is a three-electrode triggered spark-gap switch, operated at atmospheric pressure, made in-house. The capacitor bank can be charged up to 7.5 kV using a Cockroft-Walton type circuit. The discharging system and the switches were built according to [24]. The setup can provide pulsed currents up to 10 kA. The charging and discharging voltage is measured via a 1:1000 high-voltage probe with a bandwidth of 80 MHz [25] connected to a Tektronix TDS3034 oscilloscope [26]. The current pulse is measured with a commercial Rogowski coil [27] whose signal is sent to the same oscilloscope.

For the first tests, 10 pulsed currents of 4 kA peak were supplied to the coil. Figure 16 shows a typical pulse shape. Every pulse has a duration of 200 μs . After the pulsed tests had been conducted, the joints were disassembled for a visual inspection of the CuBe contacts. No visible damages were found; in particular, no melting and oxidation could be observed indicating the good sturdiness of the joints to repeated kilo-Ampere current pulses warranting the choice

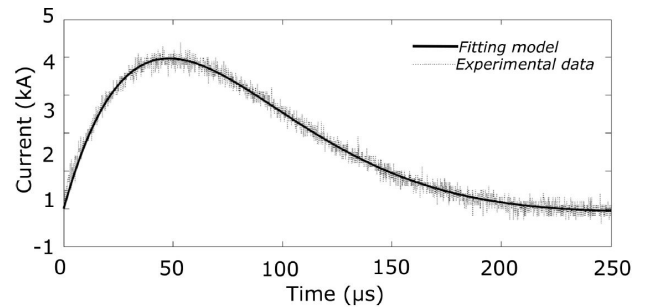


FIGURE 16. Typical current pulse recorded with the Rogowski coil. The current reaches 4 kA. Fit of the data: $I = 15.0258e^{-\alpha_1 t} \sin(\omega_1 t)$, with $\alpha_1 = 17588.9 \text{ s}^{-1}$ and $\omega_1 = 13795.3 \text{ rad/s}$.

of the contact material as well as the designs of the joint and the clamping structure.

4.2. Magnetic field

The shape and size of the coils are defined by the available space and the spatial distribution of the magnetic field for a stable plasma confinement. The complexity of their design and construction grows as the number of turns and layers increases leading to more joints. For designing a demountable coil with multi-layers and high number of turns, it is sensible to start with a relative simple coil whose turns are only a fraction of the final prototype. In the present work, a 4 turn coil with 2 layers (2 turns per layer) was proposed as a first step towards the final product, referred to as the prototype CDTCF introduced in Sec. 3. The actual coils for the TPM-1U table-top tokamak have 64 turns distributed across 8 layers. Hence, it is important to ensure that the sub-scale model of the CDTCF can supply the expected center magnetic field of the actual coil. To do so, the same principles of construction are employed to ensure that the turns and layers follow the same pattern for both the sub-scale and full-scale coils. The target of the central magnetic field for the final coil is 0.1 T so should be the sub-scale prototype. This magnitude defines the amount of current that has to flow through the winding. Here, as we guaranteed the same geometry with the sub-scale model, it allows us to check that the gauge of the chosen magnet wire is appropriate to transmit the expected current. As the sub-scale coil has less turns, it should carry more current for the same target field thereby providing a safety margin on the wire size. By increasing step by step the magnitude of the pulsed current and measuring the resulting center field, it was found that a current of 9.44 kA in the sub-scale coil can supply 0.117 T a bit larger than the specified 0.1 T. It is then expected that, in the actual coil, less current would be needed to reach such a magnitude. To obtain the current in the coil from the measurement of the center magnetic field, a semi-analytical model was used to relate the current to the field. This model can also be used to check that

the final prototype can produce the target field at lesser current. The same model was used previously in Sec. 3.3 to compute the resulting vertical force acting on the wires [see (4)]. The model incorporates some details of the geometry of the turns via a set of piecewise functions. The set defines the spatial distribution of the turns according to the parameters and coordinate system shown in Fig. 17 and 18. The functions depend on the azimuthal angle φ so that,

$$\begin{aligned} X &= r_{\text{int}} \cos(\varphi), & Y &= r_{\text{int}} \sin(\varphi), \\ Z &= h(\varphi), & 0 &\leq \varphi \leq 4\pi, \\ r_2 &= r_1 + \sqrt{\delta^2 - (z_2 - z_1)^2}, \\ Z &= h(\varphi), & 4\pi < \varphi \leq 3\pi, \\ X &= r_{\text{ext}} \cos(\varphi), & Y &= r_{\text{ext}} \sin(\varphi), \\ Z &= h(\varphi), & 3\pi < \varphi \leq 0, \end{aligned}$$

where X , Y and Z are the spatial coordinates of the points along the inner and outer helices. The angle φ goes from 0 to 4π for the inner helix (first function above, see Fig. 18) at radius r_{int} , and from 3π to 0 for the outer helix (third function) at radius r_{ext} . The second piecewise function links the first and the third functions as shown in the Fig. 17. The radius r_2 for the second function is defined through the interval $r_1 \leq r_2 \leq r_1 + \delta$. To calculate the magnetic field at any point in space, the contribution of the three piecewise functions should be taken into account [28]. Here, the interest lies in estimating the center field at the intersection of the center axis of the coil and its mid-plane (origin). The component of the field of interest is along the z axis (center axis of the coil) that is experimentally obtained from a B -dot pickup coil. The B -dot coil operates in a frequency range from low frequencies up to 200 kHz with a sensitivity β of the order of 4.5×10^{-4} V/T. Replacing the resistor in the circuit of Fig. 14 with a lesser resistance, an oscillatory current pulse is produced and detected as a voltage signal by the B -dot coil. The calibration is described in [29]. From the Biot-Savart law and approximating the conductors as filaments, the component B_z along the center axis is computed as follows,

$$B_z = \frac{\mu_0}{4\pi} \Pi_z I, \quad (6)$$

with,

$$\Pi_z = \int_0^{\frac{2\pi H}{h}} \frac{-Y(y-Y) - X(x-X)}{\left[(x-X)^2 + (y-Y)^2 + \left(z - \frac{h\varphi}{2\pi} \right)^2 \right]^{\frac{3}{2}}} d\varphi, \quad (7)$$

where \mathbf{r} is the distance from any points in the current-carrying filament to any points in space (in this particular case the origin), H is the total height of the coil and h is the helix pitch (see Fig. 18). The center field B_z is numerically integrated using the trapezoidal method.

Knowing the expression of the center magnetic field given by (6), it is then possible to extract the current I flowing through the coil. The current is given here as,

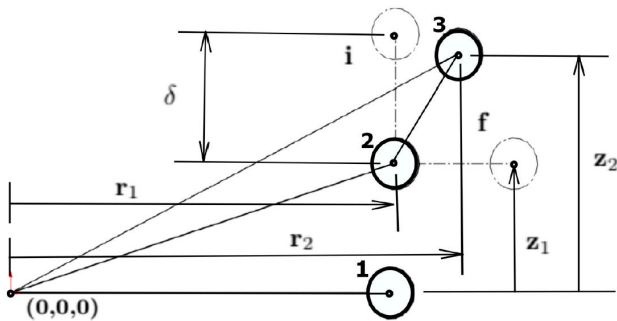


FIGURE 17. Cross section view in a vertical plane that passes through the mid-plane of the coil (right side). At point 1 and radius r_{int} . At point i , two turns have been completed. The transition from one turn to the next starts from i to finish at f sweeping $\pi/2$. The transition follows a smooth helix of variable radius up to r_{ext} then the radius is constant until the full coil path is completed.

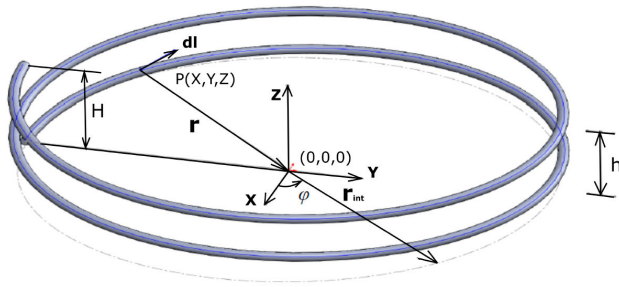


FIGURE 18. Path modeled by the first piecewise function to calculate the magnetic field contribution of all the differential lengths dl 's, with respect to the coil origin $(0, 0, 0)$ at radius r .

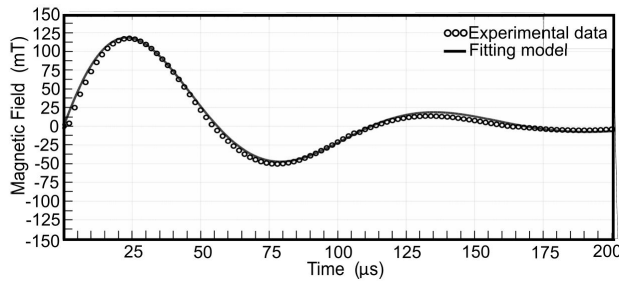


FIGURE 19. Evolution of the magnetic field response of the coil to the pulse current at the center. Fit of the data: $B = 0.174e^{-16400t} \sin(56000t)$.

$$I = \frac{4\pi B_z}{\mu_0 \Pi_z} \quad (8)$$

with $\Pi_z = 63.9$ A/m the integral found in Eq. (6). Thus, using the above relation, a measured peak field of $B_z = 49.56$ mT originates from a current pulse as shown in the Fig. 16 of 4 kA peak. As aforementioned, the target magnetic field is 0.1 T at the coil origin which requires a current of 8.071 kA according to Eq. (8). The experimental measurements gave a current of 9.44 kA for a center magnetic field of 0.117 T, a little larger than the target value. For consistency, it is checked

that the ratio of the peak current to the maximum field is linearly conserved, $8.071 \text{ kA} / 0.1 \text{ T} = 0.8071 \text{ kA/T}$ compared to $9.44 \text{ kA} / 0.117 \text{ T} \simeq 0.80684 \text{ kA/T}$ with a relative error of the order of 0.03%.

5. Conclusion

A prototype of a CDTFC for the table-top tokamak TPM-U1 was built and tested. Different steps were taken to ensure that the technical choices were sound and could be applied directly to the final coil. For the CDTFC design, a 3 mm gap between turns was filled with epoxy resin to reduce the risk of electric arcs and to avoid any relative motion between wires. Furthermore, for achieving light pressure contacts to carry current densities of at least 75 kA/cm^2 (up to 263 kA/cm^2 experimentally achieved), CuBe material was used to make conical joints. These joints are maintained in place by a straightforward clamping system with moderate fastening forces simplifying considerably the complexity of handling the CDTFC. These forces were estimated to avoid exceeding the maximum yield stress of the epoxy resin. For the proposed CDTFC prototype, the total current in the coil should amount to about 9 kA to produce about 0.1 T at its center. The resulting current density at the joints is a moderate 3.1 kA/cm^2 . These are the expected numbers for the final coil; and all the sequences presented in this work to built the 4 turn CDTFC prototype can be strictly adopted for constructing the final multi-turn target coil with CuBe / CuBe joints. The same approach can be used for any conventional demountable coils for table-top tokamak.

Acknowledgments

The authors would like to thank UNAM DGAPA for the support of the posdoctoral scholarship through the trade CJIC CTIC 5654 2022, to CONAHCYT through CVU 279374, and the Instituto Politécnico Nacional CICATA Querétaro for backup and use of laboratory.

1. C. Neumeyer *et al.*, Operational Experience with NSTX Demountable TF Joint, In *21st IEEE/NPS Symposium on Fusion Engineering SOFE* **05** (2005) pp. 1-4, <https://doi.org/10.1109/FUSION.2005.252878>.
2. G. C. Burdiak, Production and Evolution of Multiple Converging Radiative Shocks Inside Thick, Gas-Filled Cylindrical Liners, pp. 73-112 (Springer International Publishing, Cham, 2014), https://doi.org/10.1007/978-3-319-06962-3_5.
3. F. Bellina, M. Guarneri, and A. Stella, The RFX toroidal field winding design, *IEEE Transactions on Magnetics* **24** (1988) 1252, <https://doi.org/10.1109/20.11463>.
4. F. J. Mangiarotti and J. V. Minervini, Advances on the Design of Demountable Toroidal Field Coils With REBCO Superconductors for an ARIES-I Class Fusion Reactor, *IEEE Transactions on Applied Superconductivity* **25** (2015) 1, <https://doi.org/10.1109/TASC.2014.2379641>.
5. N. Mitchell *et al.*, Superconductors for fusion: a roadmap, *Superconductor Science and Technology* **34** (2021) 103001, <https://dx.doi.org/10.1088/1361-6668/ac0992>.
6. Z. Hartwig *et al.*, An initial study of demountable high-temperature superconducting toroidal field magnets for the Vulcan tokamak conceptual design, *Fusion Engineering and Design* **87** (2012) 201, <https://doi.org/10.1016/j.fusengdes.2011.10.002>.
7. A. Sagara *et al.*, Helical reactor design FFHR-d1 and c1 for steady-state DEMO, *Fusion Engineering and De-*

- sign **89** (2014) 2114, <https://doi.org/10.1016/j.fusengdes.2014.02.076>.
8. B. Sorbom *et al.*, ARC: A compact, high-field, fusion nuclear science facility and demonstration power plant with demountable magnets, *Fusion Engineering and Design* **100** (2015) 378, <https://doi.org/10.1016/j.fusengdes.2015.07.008>.
 9. G. Rolando *et al.*, Performance assessment and optimization of the ITER toroidal field coil joints, *Superconductor Science and Technology* **26** (2013) 085004, <https://dx.doi.org/10.1088/0953-2048/26/8/085004>.
 10. A. J. Creely *et al.*, Overview of the SPARC tokamak, *Journal of Plasma Physics* **86** (2020) 865860502, <https://doi.org/10.1017/S0022377820001257>.
 11. M. Lindero-Hernández, G. Ramos-López, and M. Nieto-Pérez, Evaluation of Copper-Beryllium Contacts for High Current Density Pulsed Applications, *IEEE Transactions on Plasma Science* **47** (2019) 4048, <https://doi.org/10.1109/TPS.2019.2925382>.
 12. G. Ramos, M. Lindero-Hernandez, and M. Nieto-Perez, Design and construction of demountable circular coil with high current density contacts, In 2015 IEEE Pulsed Power Conference (PPC) (2015) pp. 1-4, <https://doi.org/10.1109/PPC.2015.7296937>.
 13. M. Nieto-Perez *et al.*, Design and subsystems tests for the TPM-1U tokamak, In 2015 IEEE 26th Symposium on Fusion Engineering (SOFE) (2015) pp. 1-8, <https://doi.org/10.1109/SOFE.2015.7482286>.
 14. D. Hernández-Arriaga, D. M. Ventura-Ovalle, and M. Nieto-Pérez, Design of the Toroidal Field Coil System for the TPM-1U Tokamak, *Fusion Science and Technology* **75** (2019) 148, <https://doi.org/10.1080/15361055.2018.1554390>.
 15. O. Anderson and H. Furth, Imperfect axisymmetry in the Tokamak Configuration, *Nuclear Fusion* **12** (1972) 207, <https://dx.doi.org/10.1088/0029-5515/12/2/011>.
 16. B. Mahdavi-pour, A. S. Elahi, and M. Ghoranneviss, Effects of Resonant Helical Field on Toroidal Field Ripple in IR-T1 Tokamak, *Journal of Physics: Conference Series* **982** (2018) 012004, <https://dx.doi.org/10.1088/1742-6596/982/1/012004>.
 17. E. R. Stauffacher, *Short-time Current Carrying Capacity of Copper Wire*, **31** (1928) 326-327.
 18. S. Babic and C. Akyel, Magnetic force between inclined circular loops (Lorentz approach), *PIER B* **38** (2012) 333, <https://doi.org/10.2528/PIERB12011501>.
 19. M. Abramowitz and I. A. Stegun, eds., *Handbook of Mathematical Functions with Formulas, Graphs, and Mathematical Tables*, Tenth printing ed. (U.S. Government Printing Office, Washington, DC, USA, 1972).
 20. I. S. Gradshteyn and I. M. Ryzhik, *Table of integrals, series, and products*, Seventh ed. (Elsevier/Academic Press, Amsterdam, 2007), p. xlvi.
 21. P. H. Titus, PSFC / JA-039 *Structural Design of High Field Tokamaks* (2003) <https://api.semanticscholar.org/CorpusID:2516542>.
 22. H. N. Jones *et al.*, Pulsed Current Static Electrical Contact Experiment, *IEEE Transactions on Magnetics* **43** (2007) 343, <https://doi.org/10.1109/TMAG.2006.887716>.
 23. C. Neumeyer *et al.*, NSTX TF joint failure and re-design, In 20th IEEE/NPSS Symposium on Fusion Engineering (2003) pp. 35-38, <https://doi.org/10.1109/FUSION.2003.1425872>.
 24. H. Bluhm, *Switches*, pp. 83-133 (Springer Berlin Heidelberg, Berlin, Heidelberg, 2006), https://doi.org/10.1007/3-540-34662-7_4.
 25. North Star High Voltage, Rose Loop NE, Bainbridge Island, WA, USA., Internet source: <https://www.highvoltageprobes.com/>.
 26. Tektronix, SW Karl Braun Drive, Tektronix, Inc., Beaverton, OR, USA., Internet source: <https://www.tek.com/en>.
 27. P. Electronics, 4009 Transport St., Palo Alto, CA94303, USA., Internet source: <https://www.pearsonelectronics.com/>.
 28. T. Tominaka, Analytical field calculations for various helical conductors, *IEEE Transactions on Applied Superconductivity* **14** (2004) 1838, <https://doi.org/10.1109/TASC.2004.830878>.
 29. M. L. Hernandez, *et al.*, Design and construction of a single axis, low-frequency magnetic probe (B-dot probe) calibrated with a LCvar Helmholtz resonant circuit, *Rev. Mex. Fis.* **65** (2019) 560-565, <https://doi.org/10.31349/RevMexFis.65.560>.